

Conference Paper

Experimental performance analysis of advanced layers for electronic circuit boards

Klarmann, S., Vagapov, Y. and Gotzig, H.

This is a paper presented at the *54th IEEE Int. Universities Power Engineering Conference UPEC-2019*, Bucharest, Romania, 3-6 Sept. 2019. Copyright of the author(s). Reproduced here with their permission and the permission of the conference organisers.

Recommended citation:

Klarmann, S., Vagapov, Y. and Gotzig, H. (2019) 'Experimental performance analysis of advanced layers for electronic circuit boards'. In: *Proc. 54th IEEE Int. Universities Power Engineering Conference UPEC-2019*, Bucharest, Romania, 3-6 Sept. 2019, pp. 1-4. doi: 10.1109/UPEC.2019.8893441

Experimental Performance Analysis of Advanced Layers for Electronic Circuit Boards

Steffen Klarmann

Faculty of Art, Science and Technology
Glyndwr University
Wrexham, UK

Yuriy Vagapov

Faculty of Art, Science and Technology
Glyndwr University
Wrexham, UK

Heinrich Gotzig

Valeo S.A.
Bietigheim-Bissingen, Germany

Abstract—This paper provides an experimental performance analysis of advanced layers for electronic circuit boards. The base material of the advanced layers used in the experiments is Al-5052, with the dimensions of 100mm x 20mm x 1mm. As insulating material between the base and conductor, two aluminium coatings were investigated and the surface structure and thermal conductivity of the coatings were examined. Furthermore, three electro-conductive adhesives were applied onto the coatings. Initially, electrical performance is investigated and electrical components were applied onto the new surface structure. Finally, the environmental tests were performed to determine the robustness of the evaluated system.

Keywords—aluminium; electro conductive adhesive; coating; plasma anoxided, insulated-metal-substrate

I. INTRODUCTION

Power density of electronic equipment has significantly increased over the past decades and has brought new challenges in thermal management of electronic components. In terms of PCB design, it has required the introduction and implementation of new technologies and materials aimed to ensure efficient heat transfer. The appropriate temperature of lightning devices installed on PCBs, such as high power LEDs, is a crucial factor affecting on the device's operation. A higher operational temperature of the junction reduces LED life time and reliability and can produce a colour shift. Hence, the improvement in the PCB thermal management for various LED applications is strongly desired to avoid issues relating to the higher temperature. In this paper two different approaches to increase the thermal performance of PCB technologies have been investigated.

As a result of high-power electronic components, improvements on FR4 based PCBs have been widely studied. By adding a heat sink on the back of the FR4 based PCBs, their thermal performance is improved. However, by implementing thermal vias, which are metal based through-holes, heat transfer is enhanced [6]. Furthermore, lower thermal resistance was accomplished by a reduction of pitch size, increasing the number of copper layers and the barrel thickness of the vias [7]. In recent studies, inorganic dielectric-layer-coated MCPCBs were investigated. Compared to the regular ceramic polymer composite film, dense aluminium film was deposited. Comparing thermal resistance of the conventional dielectric layer to this approach, an improvement of 4-5 K/W was achieved. Concluding that the thermal performance of dielectric layer in the MCPCB had been improved [1]. Moreover, by

changing the common DLC, AlN, Al₂O₃ or BeO dielectric fillers to diamond powdered filler material, the thermal resistance will decrease. In addition, a flat plane heat pipe will enhance thermal performance of MCPCBs [5]. Flip-chip technology was widely investigated to improve the thermal performance [3]. Due to the connection of the device on the reverse side, emitting photons are no longer impaired by front-side connections like wires or bonding pads. Consequently, a higher output power of the flip-chip was achieved [4]. In addition, thermal performance was improved by using this technology. New electrolysis and electroplating technique was proposed to reduce junction temperature of LEDs. By adding Ni/Au on an electroplating copper, a significant reduction of LED junction temperature was achieved. Hence, by using EET, the luminous intensity was increased [2]. By adding Ag reflector mirrors to the reverse side of the flip-chip based LEDs, two major issues of LEDs (reliability and power output) were improved. Compared to conventional non flip-chip LEDs, flip-chip LEDs have a much shorter thermal path [3].

It has been reported that using graphite-based TIM a reduction of peak temperature in 3D IC layers of 12.84% compared to mono layer Graphene was achieved [8]. Graphene volume ratios (V_G) is crucial for the improvement of thermal conductivity. [9] has shown that by changing V_G from 30% to 75% an increase of ≈ 1200 W/m²·K was achieved. Concluding that graphene enhanced TIM can reach through plane thermal conductivity up to 1000 W/m²·K, whereas in plane thermal conductivity up to 5000 W/m²·K can be reached [10].

II. COATINGS

In this paper, two aluminium coatings are investigated. In a first step, coatings are applied onto Al-5052 with a dimension of 100mm×20mm×1mm. However, thickness is determined at total thickness of coating, whereas only 50% is added to the top of aluminium substrate.

A. Surface Structure

SEM (scanning electron microscope) and optical microscope were used to take pictures to analyse the surface structure of the coatings. Additionally, an optical microscope and SEM was also used on raw Al-5052. This investigation was done initially with an optical microscope and at a next step with a LEO 430 scanning electron microscope. The resolution is 5nm and the maximum magnification of 300,000. REM image was taken at a magnification level of 500, Fig. 1 shows the images.

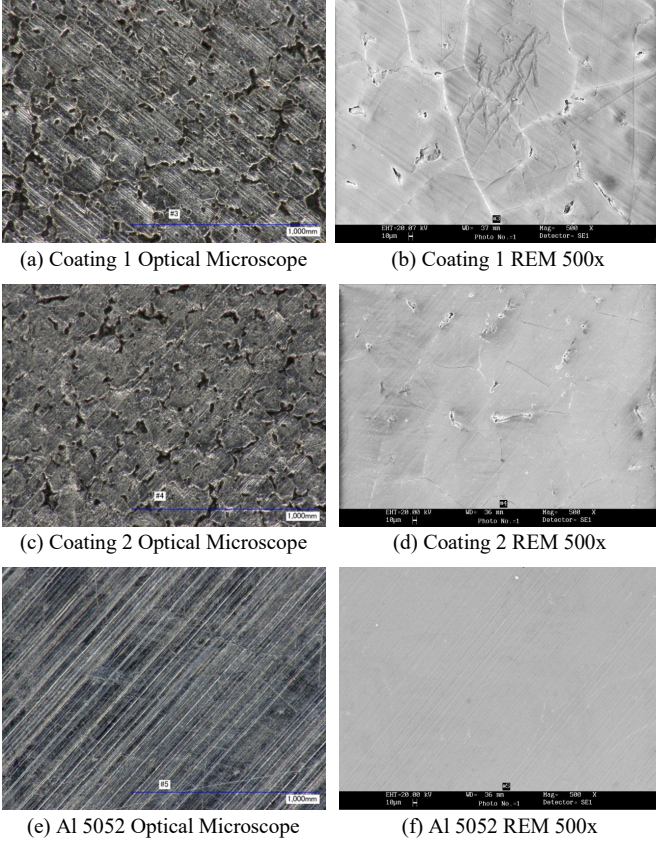


Fig. 1. Coating overview.

B. Thermal Conductivity

Measurement of thermal conductivity was conducted in high-vacuum at an absolute pressure of $\approx 1 \times 10^{-4}$ mBar and an ambient temperature of 25°C. At the first step, periodic current $I = I_0 \cos \omega t$ was applied. Therefore,

$$P = I^2 R = \frac{I_0^2 R}{2} (1 + \cos 2\omega t) \quad (1)$$

where I_0 is amplitude peak of current in nominal heater at frequency ω and R_0 is nominal heater resistance.

Thermal wave results in thermal oscillation in resistor, hence:

$$\Delta \tilde{T} \frac{d}{dt} = \Delta T_0 \cos(2\omega t + \varphi) \quad (2)$$

where ΔT_0 is described as temperature difference from initial condition to steady-state and φ is the phase angle between oscillating angles.

Thermal oscillation results in resistance oscillation, therefore:

$$R = R_0 (1 + \beta \Delta T) = R_0 + R_0 \beta \Delta T_0 \cos(2\omega t + \varphi) \quad (3)$$

where R and R_0 describe resistance of metal line at temperature T_0 and $T_0 + \Delta T$, β is the temperature coefficient of resistance.

The amplitude and phase of the diffusion wave depends on the thermal conductivity, thermal capacity and frequency. The measured voltage at the resistor depends on a base frequency and the appropriate second harmonic:

$$U = I_0 R_0 \cos \omega t + \frac{I_0 R_0 \beta \Delta T_0}{2} [\cos(3\omega t + \varphi) + \cos(\omega t + \varphi)] \quad (4)$$

In conclusion, the complex thermal wave is described as follows [11], [12]:

$$\Delta T = \frac{P}{l\pi\lambda} \left(-\frac{1}{2} \ln \omega + k \right) \quad (5)$$

where P/l is the amplitude of the power per unit length in line source of heat, λ is thermal conductivity of an infinite half-volume and k is a frequency independent complex constant.

Therefore, the thermal conductivity is described as the gradient of the real part as a function of the logarithmic frequency, with

$$d(\Delta T_0) = \frac{2(U_{3\omega 1} - U_{3\omega 2})}{l_0 R_0 \beta} \quad (6)$$

where $U_{3\omega 1}$ is the voltage at the third harmonic for a frequency f_1 and $U_{3\omega 2}$ the voltage at the third harmonic for frequency f_2 respectively.

$$d(\ln \omega) = \ln \frac{f_2}{f_1} \quad (7)$$

$$\frac{d(\Delta T)}{d(\ln \omega)} = -\frac{1}{2} \frac{P}{l\pi\lambda} \quad (8)$$

Hence, thermal conductivity is described as follows:

$$\lambda = \frac{U^3 \ln \left(\frac{f_2}{f_1} \right)}{4\pi l R^2 (U_{3\omega 1} - U_{3\omega 2})} \frac{dR}{dT} \quad (9)$$

In conclusion, the coating 1 results in a thermal conductivity of 1.88 W/m·K and a total thickness of 15 μm , whereas coating 2 results in a thermal conductivity of 1.54 W/m·K and a total thickness of 25 μm .

III. ADHESIVE

Adhesives are examined to determine performance in terms of electrical conductivity, dosing capability and environmental robustness. Therefore, three adhesives are investigated. All adhesives are 1-component and use Ag as filler. In a next step, electrical resistance is examined. Adhesive is applied with a Preeflow eco-PEN300 and a Vieweg DC200 dispenser to FR-4 base material. Preeflow eco-PEN operating pressure range is from 0 to 6 bar, an approximate dosing volume per revolution of 0.012 ml/rev and a volume flow range from 0.12-1.48 ml/min. Vieweg DC200 dispenser has a flow rate range from 0.5-6.0 ml/min

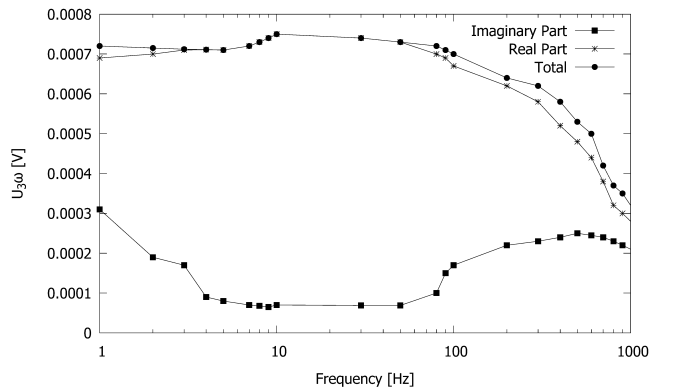


Fig. 2. Thermal conductivity measurement coating 1.

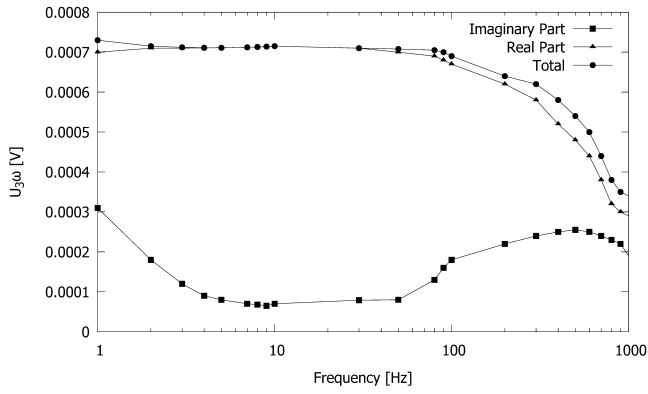


Fig. 3. Thermal conductivity measurement coating 2.

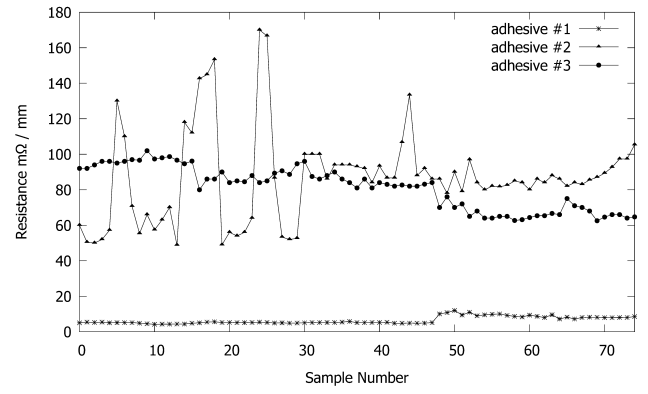


Fig. 4. Adhesive electrical resistance.

and a minimum dispensing volume of 0.004 ml. Vieweg TESeries needles with a diameter 0.33mm were used to dose adhesive. The dispenser is mounted onto a KUKA KR30HA robot, with a positioning accuracy of 0.02mm. However, the distance from needle to the substrate was 1.8mm, whereas the speed of robot was at 3 mm/s, the ambient temperature was at 27°C and the humidity at 46% RH. Table I shows an overview of investigated adhesives, and Fig. 4 the analysis result.

IV. APPLICATION OF COMPONENTS

After the base material, insulating layer and the electroconductive adhesive are applied and the electronic components are mounted onto the structure. Seven surface mounted light-emitting diodes, one negative temperature coefficient resistor and a connector are also installed onto the PCB. The package of SMD LEDs is ceramic based, with a maximum operating temperature range from -40°C to +125°C, forward current from 50mA to 1.500mA with a surge current of 2.500mA, maximum thermal resistance junction/solder joint 7.3 K/W and a typical luminous intensity of 110.6 cd. The solder pad material of the light-emitting-diode is NiPdAu with a copper lead frame. The resistance at the temperature of 25°C of NTC is 10kΩ, and the tolerance is at ±1% with the maximum operating temperature range between -40°C to +125°C. In addition, the connector is a 4 pin model, and the pins are Au over Ni and the PCB connector Cu over Ni. All of the electronic components are applied onto adhesive with KUKA KR30HA robot with a Vectra ASM ceramic pipette. Due to the requirements, AOI was programmed to achieve the required precision. The AOI was developed using National Instruments Vision Builder and a gigEPRO camera GP2239M. The resolution of the monochrome CMOS camera used is 1920×1080 pixel, the sensor size is 1/1.2" and the pixel size is 5.85μm×5.85μm. After the components are applied onto the electro-conductive adhesive, curing is required at a temperature of 175°C, for a curing duration of 5 minutes.

TABLE I. ADHESIVE OVERVIEW

#	Density [g/cm ³]	Particle Size [μm]	Viscosity [mPa·s]	Basis
1	5.3	< 3	35,000	Epoxy
2	2.4	20	100,000	Epoxy
3	4.1	20	80,000	Epoxy

V. ENVIRONMENTAL TESTS

At the first stage, the coatings are applied onto Al-5052 base material, followed by three electro-conductive adhesives. Therefore, 6 elaborations are available for each testing scenario. Elaboration 1 and 2 are based on adhesive 1 with coating 1 and 2, elaboration 3 and 4 are based on adhesive 2, corresponding coating 1 and 2, whereas elaboration 5 and 6 are based on adhesive three with coating 1 and 2. 20 samples of each elaboration have been produced for the analysis. This results in a total of 120 samples. At the next stage, LEDs, NTC and the connector are applied onto each sample. However, the environmental tests are divided on the one hand into thermal shock tests and on the other hand into humidity tests. Resulting in 10 samples being investigated per test. During the thermal shock tests, the samples are placed into a climate chamber with two

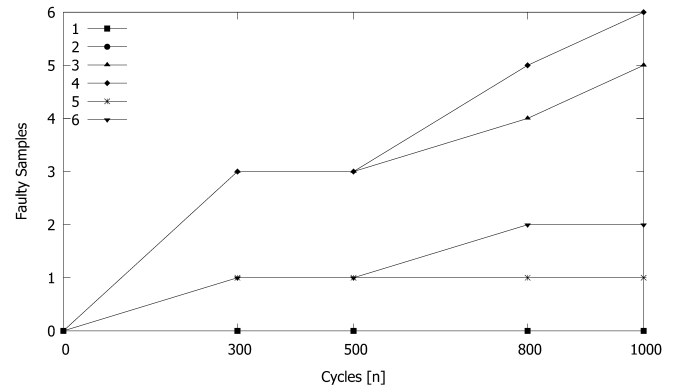


Fig. 5. Failure rates thermal environmental test.

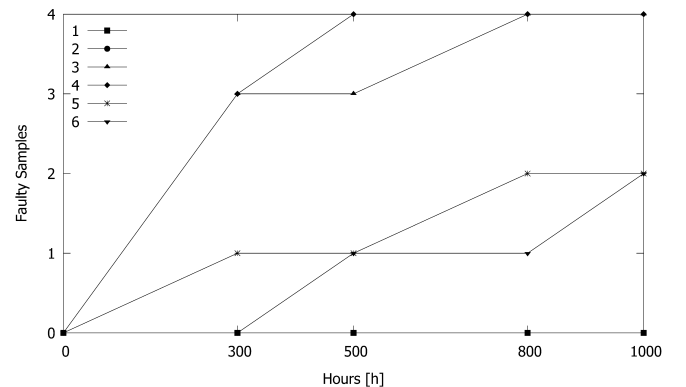


Fig. 6. Failure rates humidity environmental test.

temperatures. In the top chamber, the temperature is set to 85°C, whereas in the bottom chamber it is set to -40°C. The duration for the samples in both areas is 40 minutes; afterwards the transfer to other chamber is done within 30 seconds. The duration of the temperature shock test lasts for 1000 cycles.

The humidity tests were performed using the climate chamber where the temperature was set to a constant value of 85°C and the humidity set to a constant 90%rH. Afterwards, functional testing was performed at $U = 20V$ and $I = 50mA$. The first functional testing of LEDs was done after 300 cycles for temperature shock corresponding 300 hours for humidity testing. The subsequent functional tests were performed at 500 cycles, 800 cycles and 1000 cycles for temperature shocks, corresponding to 500 hours, 800 hours and 1000 hours for humidity tests. The results of the functional tests for the thermal environment are depicted in Fig. 5, whereas the functional test results for humidity testing is illustrated in Fig. 6.

VI. CONCLUSION

In this paper, two aluminium coatings have been investigated with regard to the surface structure and the thermal conductivity of the coatings. Also, three electro conductive adhesives have been examined to determine the electrical resistance on the FR-4 sample. Finally, electro conductive adhesive has been applied onto the coatings and environmental tests have been performed. It can be seen, that a low particle size results in a robust process of applying adhesive onto a substrate. In contrast, larger particles lead to a more difficult application process, where constant electrical resistance of the system cannot be guaranteed. In addition, the aluminium coating has been evaluated, it has been shown, that the thickness of the aluminium did not affect the results of environmental tests. The analysis of the environmental tests showed that the adhesive 1 applied on coating 1 and coating 2 resulted in zero failures in both temperature shock and humidity tests whereas adhesive 2 applied on coating 3 and coating 4 resulted in the highest failure rate.

REFERENCES

- [1] H.M. Cho, and H.J. Kim, "Metal-core printed circuit board with alumina layer by aerosol deposition process," *IEEE Electron Device Letters*, vol. 29, no. 9, pp. 991-993, Sept. 2008. doi:10.1109/led.2008.2001633
- [2] K.C. Chen, Y.K. Su, C.L. Lin, et al., "Thermal management and novel package design of high power light-emitting diodes," in *Proc. 58th Electronic Components and Technology Conference*, Lake Buena Vista, USA, 27-30 May 2008, pp. 795-797. doi:10.1109/ectc.2008.4550065
- [3] W.S. Chen, S.C. Shei, S.J. Chang, et al., "Rapid thermal annealed InGaN/GaN flip-chip LEDs," *IEEE Transactions on Electron Devices*, vol. 53, no. 1, pp. 32-37, Jan. 2006. doi:10.1109/ted.2005.860760
- [4] J.J. Wierer, D.A. Steigerwald, M.R. Krames, et al., "High-power AlGaInN flip-chip light-emitting diodes," *Applied Physics Letters*, vol. 78, no. 22, pp. 3379-3381, 2001. doi:10.1063/1.1374499
- [5] S. Shen, H. Huang, and H. Shaw, "Design and estimation of a MCPCB-flat plate heat pipe for LED array module," in *Proc. IEEE Int. Conf. on Mechatronics and Automation*, Takamatsu, Japan, 4-7 Aug. 2013, pp. 158-163. doi:10.1109/icma.2013.6617910
- [6] S. Andreev, N. Spasova, and D. Chikurtev, "Investigations on heat extraction in multilayer PCB structures," in *Proc. 27th IEEE Int. Sci. Conf. Electronics - ET2018*, Sozopol, Bulgaria, 13-15 Sept. 2018, pp. 1-4. doi:10.1109/ET.2018.8549638
- [7] D. Gautam, D. Wager, F. Musavi, M. Edington, W. Eberle, and W. G. Dunford, "A review of thermal management in power converters with thermal vias," in *Proc. 28th Annual IEEE Applied Power Electronics Conference and Exposition (APEC)*, Long Beach, USA, 17-21 March 2013. pp. 627-632, doi:10.1109/APEC.2013.6520276
- [8] S.K. Vendra, and M. Chrzanowska-Jeske, "Thermal management in 3D IC designs for nano-CMOS technologies: Analysis on graphene vs. graphite-based TIM," in *Proc. 13th IEEE Nanotechnology Materials and Devices Conference*, Portland, USA, 14-17 Oct. 2018, pp. 1-4. doi:10.1109/NMDC.2018.8605929
- [9] N. Wang, S. Chen, A. Nkansah, Q. Wang, X. Wang, M. Chen, L. Ye, and J. Liu, "Vertically aligned graphene-based thermal interface material with high thermal conductivity," in *Proc. 24th Int. Workshop on Thermal Investigations of ICs and Systems - THERMINIC*, Stockholm, Sweden, 26-28 Sept. 2018, pp. 1-4. doi:10.1109/THERMINIC.2018.8593303
- [10] A.A. Balandin, S. Ghosh, W. Bao, I. Calizo, D. Teweldebrhan, F. Miao, and C.N. Lau, "Superior thermal conductivity of single-layer graphene," *Nano Letters*, vol. 8, no. 3, pp. 902-907, 2008. doi:10.1021/nl0731872
- [11] D. Cahill, and R. Pohl, "Thermal conductivity of amorphous solids above the plateau," *Physical Review B*, vol. 35, no. 8, pp. 4067-4073, 1987. doi:10.1103/physrevb.35.4067
- [12] D. Cahill, "Thermal conductivity measurement from 30 to 750 K: the 3ω method," *Review of Scientific Instruments*, vol. 61, no. 2, pp. 802-808, 1990. doi:10.1063/1.1141498